



6-phosphofructo-2-kinase/fructose-2,6-bisphosphatase Suppresses Neuronal Apoptosis by Increasing Glycolysis and “cyclin-dependent kinase I-Mediated Phosphorylation of p27 After Traumatic Spinal Cord Injury in Rats

Liansheng Gao^{1,*}, Chun Wang^{1,*}, Bing Qin^{1,*}, Tao Li¹, Weilin Xu¹, Cameron Lenahan², Guangyu Ying¹, Jianru Li¹, Tengfei Zhao³, Yongjian Zhu¹, and Gao Chen¹ 

Cell Transplantation
Volume 29: 1–14
© The Author(s) 2020
Article reuse guidelines:
sagepub.com/journals-permissions
DOI: 10.1177/0963689720950226
journals.sagepub.com/home/ctj


Abstract

Apoptosis is a vital pathological factor that accounts for the poor prognosis of traumatic spinal cord injury (t-SCI). The 6-phosphofructo-2-kinase/fructose-2,6-bisphosphatase (PFKFB3) is a critical regulator for energy metabolism and proven to have antiapoptotic effects. This study aimed to investigate the neuroprotective role of PFKFB3 in t-SCI. A compressive clip was introduced to establish the t-SCI model. Herein, we identified that PFKFB3 was extensively distributed in neurons, and PFKFB3 levels significantly increased and peaked 24 h after t-SCI. Additionally, knock-down of PFKFB3 inhibited glycolysis, accompanied by aggravated neuronal apoptosis and white matter injury, while pharmacological activation of PFKFB3 with meclizine significantly enhanced glycolysis, attenuated t-SCI-induced spinal cord injury, and alleviated neurological impairment. The PFKFB3 agonist, meclizine, activated cyclin-dependent kinase I (CDK1) and promoted the phosphorylation of p27, ultimately suppressing neuronal apoptosis. However, the neuroprotective effects of meclizine against t-SCI were abolished by the CDK1 antagonist, RO3306. In summary, our data demonstrated that PFKFB3 contributes robust neuroprotection against t-SCI by enhancing glycolysis and modulating CDK1-related antiapoptotic signals. Moreover, targeting PFKFB3 may be a novel and promising therapeutic strategy for t-SCI.

Keywords

PFKFB3, meclizine, neuronal apoptosis, glycolysis, traumatic spinal cord injury

Introduction

Traumatic spinal cord injury (t-SCI) is one of the most serious injuries worldwide, which can lead to a series of physiological dysfunctions, including motor and sensory impairment, chronic pain, respiratory and cardiovascular alterations, neurogenic bowels, neurogenic bladder, and even psychological disorders^{1,2}. The pathogenesis of t-SCI is complicated; it consists of primary trauma followed by secondary damage, further aggravating the injury. The primary injury quickly causes acute, mechanical destruction to the spinal cord tissues, including axons, blood vessels, and cells at the injury site³. The secondary injury is initiated after the primary insult and progresses throughout the entire

¹ Department of Neurosurgery, Second Affiliated Hospital, School of Medicine, Zhejiang University, Hangzhou, Zhejiang, China

² Burrell College of Osteopathic Medicine, Las Cruces, NM, USA

³ Department of Orthopedics, Second Affiliated Hospital, School of Medicine, Zhejiang University, Hangzhou, Zhejiang, China

* These authors contributed equally to this article as co-first authors

Submitted: September 7, 2019. Revised: February 25, 2020. Accepted: July 27, 2020.

Corresponding Authors:

Gao Chen, and Yongjian Zhu, Department of Neurosurgery, Second Affiliated Hospital, School of Medicine, Zhejiang University, 88 Jiefang Road, Hangzhou, Zhejiang 310009, China.

Emails: d-chengao@zju.edu.cn; neurosurgery@zju.edu.cn



period of injury⁴. Various mechanisms are associated with the secondary injury, including hemorrhage, ischemia, oxidative stress, inflammation, death of neurons and glia, axonal demyelination and degeneration, extracellular matrix remodeling, and gliosis^{5–8}. Additionally, neuronal apoptosis plays a critical role in contributing to the behavioral dysfunction⁹. As a result, multiple drugs aiming to reduce neuronal apoptosis may contribute to improved neurological outcomes following t-SCI¹⁰. However, the underlying mechanism of neuronal apoptosis has not yet been fully elucidated, and the curative effects are still poor¹¹.

The enzyme 6-phosphofructo-2-kinase/fructose-2,6-bisphosphatase (PFKFB) is a bifunctional enzyme that is involved in the regulation of glucose metabolism¹². The PFKFB family contains four types of isozymes, PFKFB 1–4¹³. PFKFB3 is the most studied isoform and can catalyze the synthesis of the allosteric activator, fructose-2,6-bisphosphate (F2,6BP). Increased F2,6BP promotes glycolytic flux by activating the key glycolytic enzyme, phosphofructokinase 1 (PFK1), which is important for lactate production, whereas decreased F2,6BP levels inhibit glycolysis. As a result, PFKFB3 is considered a critical stimulator of glycolysis¹². Previous studies have suggested that there is enhanced expression of PFKFB3 in rapidly proliferating transformed cells¹⁴, solid tumors, and leukemias^{14–16}. Cancer cells preferentially utilize glycolysis, rather than the citric acid cycle, as their source of energy, and this is known as the Warburg effect¹⁷. This allows the tumor cells to quickly utilize glucose, providing energy and materials for enhanced tumor proliferation¹⁸ or the prevention of apoptosis¹⁹. As a result, PFKFB3 exerts critical antiapoptotic effects toward cancer cells. PFKFB3 is also expressed on, and functions in, various cell types other than cancer cells²⁰. The enhancement of glycolysis was also identified in multiple neurological diseases, such as cerebral ischemia²¹, neurodegenerative diseases^{22,23}, traumatic brain injury²⁴, and SCI²⁵. Previous studies have indicated that increased glycolysis may provide a potential source of energy for the central nervous system (CNS), which could rescue the nerve cells²⁴. Others have indicated that glycolysis impairment induced by PFKFB3 inhibition may lead to metabolic disturbance and neuronal apoptosis²².

Other than promoting glycolysis and, therefore, protecting against apoptosis, PFKFB3 can also transfer into the nucleus and increase the content of nuclear F2,6BP. Nuclear F2,6BP is an activator of cyclin-dependent kinase 1 (CDK1), which could then promote the phosphorylation and further ubiquitination degradation of p27. p27 is a potent blocker of the G1/S transition and an activator of apoptosis. As a result, PFKFB3 may exert antiapoptotic effects by downregulating nuclear p27²⁶. In fact, this effect is far greater than the effect on promoting glycolysis.

Meclizine has been used clinically for many years, as it is a well-tolerated antihistamine agent used for the management of vertigo and motion sickness²⁷. Recently, meclizine has demonstrated neuroprotective effects on ischemic

stroke²⁸ and neurodegenerative diseases, such as Parkinson's²⁹ and Huntington's³⁰ diseases. The neuroprotective mechanisms of meclizine may rely on its ability to modulate energy metabolism, such as enhancing glycolysis and converting the method of cellular energy metabolism from mitochondrial respiration to glycolysis by increasing the PFKFB3 levels²⁹. However, whether the neuroprotective effect of meclizine-induced PFKFB3 has increased functions in t-SCI is currently unknown, and relating studies have been lacking, until now. We hypothesize that meclizine as a potential therapeutic agent paired with its target, PFKFB3, plays an important role in suppressing neuronal apoptosis in a rat model of t-SCI. The potential mechanisms may function by increasing glycolysis and promoting CDK1-mediated phosphorylation of p27.

Materials and Methods

Animals

Male Sprague Dawley rats, each weighing 250–300 g, used in this study were purchased from SLAC Laboratory Animal Co. Ltd (Shanghai, China). The animals were maintained in an environment under a constant temperature ($22 \pm 1^\circ\text{C}$) and humidity ($60 \pm 5\%$) with a 12-h light/dark cycle.

t-SCI Model

A spinal cord compressive model of t-SCI was recreated, according to the previous description³¹. In brief, the T10 vertebrae of the rats were exposed, and a laminectomy was conducted to reveal the spinal cord. A vascular clip (30 g force, INS 14120, Kent Scientific, Torrington, CT, USA) was then used to clamp the spinal cord for 30 s to create a compressive injury. The rats in the sham group received the same operation but without the clamp.

Drug and Small Interfering RNA Administration

Meclizine (100 mg/kg, Macklin, Shanghai, China), dissolved in 5 ml of normal saline, was administered to the rats via intraperitoneal injection²⁸ 1 h after t-SCI³². A mixture, consisting of two types of specific small interfering RNA (siRNA) to target the rat PFKFB3 mRNA (Genomeditech, Shanghai, China) at a dosage of 500 pmol, was prepared and dissolved in 10 μl EntransterTM in vivo transfection reagent (Engreen Biosystem, Beijing, China), and then intrathecally injected into the rats 48 h before t-SCI. The scramble siRNA was administered to the rats following the same process³³. RO3306 (4 mg/kg, Selleck Chemicals, Houston, TX, USA) was administered to the rats via oral gavage³⁴ 1 h after t-SCI^{32,35}.

Intrathecal Injection

Intrathecal injections were conducted using Hylden's method, according to the previous description³⁶. In brief, a

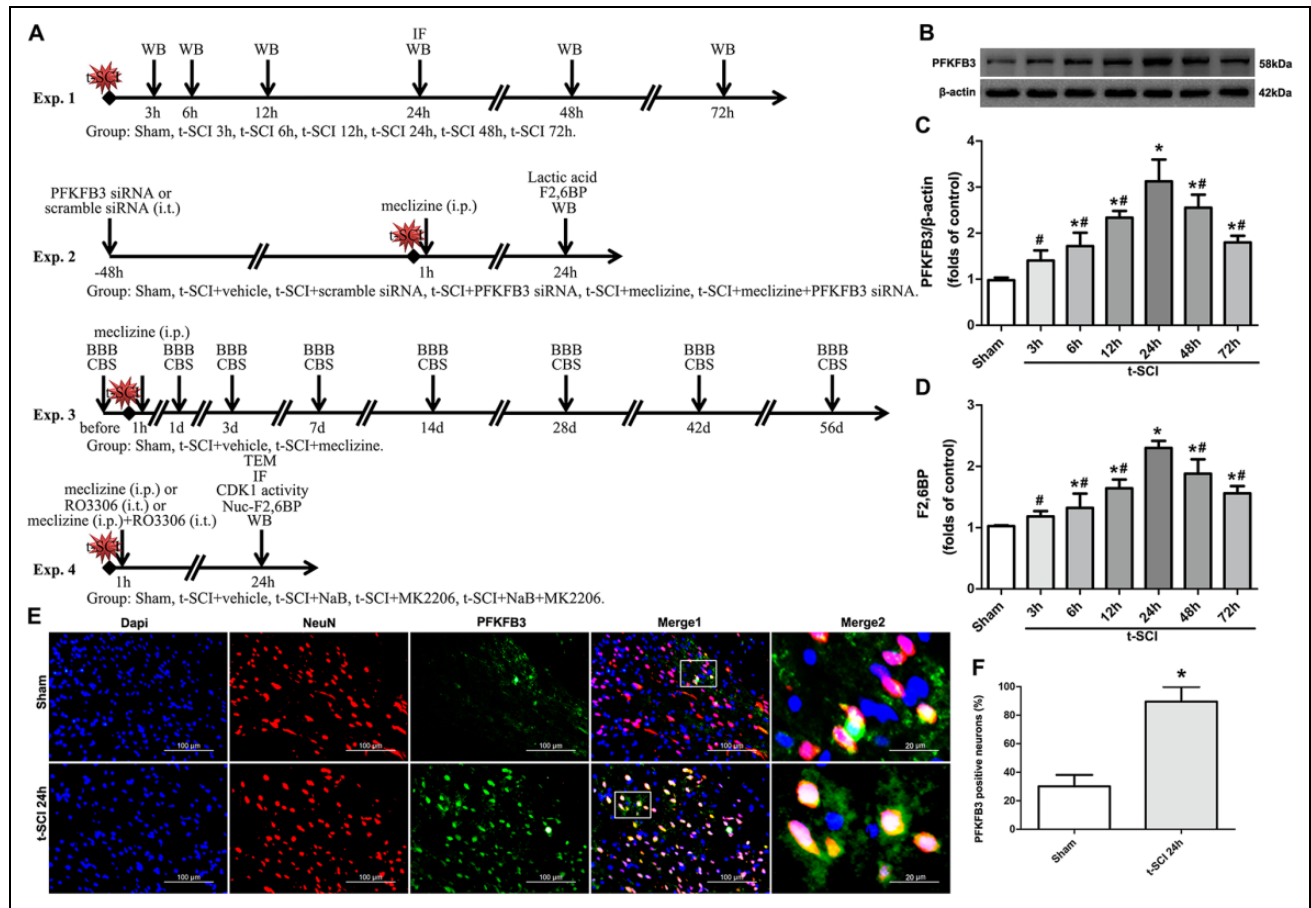


Fig. 1. Experimental designs (A). The time course of PFKFB3, and F2,6BP showed that the levels of PFKFB3 and F2,6BP were significantly elevated at 6 h, peaked at 24 h, and then significantly decreased after 24 h postinjury. Representative western blot images (B); the levels of PFKFB3 (C); and the levels of F2,6BP (D). The expression of PFKFB3 in neurons was increased at 24 h postinjury. Representative microphotographs of double immunofluorescence of PFKFB3 and NeuN (E); the proportion of PFKFB3-positive neurons (F). $N = 6$ for each group. Data are expressed as the mean \pm SD. * $P < 0.05$ versus sham; # $P < 0.05$ versus t-SCI 24 h. F2,6BP: fructose-2,6-bisphosphate; PFKFB3: 6-phosphofructo-2-kinase/fructose-2,6-bisphosphatase; SD: standard deviation.

rat was held in one hand with the back bulged, and a lumbar puncture was conducted using a microsyringe to penetrate the intervertebral space between the L5 and L6 vertebrae. A total of 10 μ l of the drug was injected at a rate of 2 μ l/min. The syringe was securely positioned for 10 min and then removed. The sham rats underwent the same procedure without drug administration.

Experimental Designs

Experiment 1. Rats were randomly divided into seven groups: sham, t-SCI 3 h, t-SCI 6 h, t-SCI 12 h, t-SCI 24 h, t-SCI 48 h, and t-SCI 72 h. Western blotting was performed in each group, while immunofluorescence staining was performed in the sham and t-SCI 24 h groups.

Experiment 2. Rats were randomly divided into six groups: sham, t-SCI + vehicle, t-SCI + scramble siRNA, t-SCI + PFKFB3 siRNA, t-SCI + meclizine, and t-SCI + meclizine

+ PFKFB3 siRNA. Then, 24 h after t-SCI, western blotting was performed. The F2,6-BP and lactic acid levels were measured in each group.

Experiment 3. Rats were randomly assigned into three groups: sham, t-SCI + vehicle, and t-SCI + meclizine. Basso, Beattie, and Bresnahan (BBB) and combined behavioral scores (CBS) were evaluated before treatment and on the 1st, 3rd, 7th, and 14th day, as well as every 2 weeks following treatment until the eighth week.

Experiment 4. Rats were randomly assigned to five groups: sham, t-SCI + vehicle, t-SCI + meclizine, t-SCI + RO3306, and t-SCI + meclizine + RO3306. Then, 24 h after t-SCI, western blotting, immunofluorescence staining, and transmission electron microscopy (TEM) were performed. CDK1 activity and nuclear F2,6-BP were also tested in each group.

Detailed experimental designs are shown in Fig. 1A.

Motor Function Assessment

The neurologic functions were evaluated by two well-trained researchers who were blinded to the groups and used the BBB scores and CBS, as previously reported³⁷.

Western Blotting

A spinal cord segment, 0.5 cm in length, from where the injured site was centered was used for protein quantification using western blotting. Proteins of the nucleus and cytosol were extracted using the NE-PER Nuclear and Cytoplasmic Extractions Kit (Thermo Fisher Scientific, Waltham, MA, USA), following the manufacturer's instructions. The protein mixture extracted from each segment was separated via electrophoresis and transferred to the polyvinylidene difluoride membrane (Bio-Rad Laboratories, Hercules, CA, USA). The membranes were first incubated with PFKFB3 (1:5,000, ab181861, Abcam, Cambridge, UK), Bax (1:1,000, ab32503, Abcam), Bcl-2 (1:500, ab59348, Abcam), cleaved caspase-3 (CC-3, 1:500, ab13847, Abcam), p-CDK1 (1:1,000, ab201008, Abcam), p27 (1:5,000, ab32034, Abcam), H3 (1:5,000, ab1791, Abcam), myelin basic protein (MBP) (1:1,000, ab209328, Abcam), APP (1:1,000, ab32136, Abcam), β -actin (1:5,000, ab8226, Abcam), and p-p27 (1:1,000, ab75908, Abcam) antibodies at 4°C overnight, respectively, and incubated with the secondary antibodies (1:10,000, ZB-2301 or ZB-2305, Zhongshan Gold Bridge, Beijing, China) at 25°C for 1 h. The proteins were detected using an ECL kit (Immobilon, Millipore, Billerica, MA, USA). The gray values of each band were calibrated according to the internal reference and compared to those of the sham group to acquire a relative value.

Immunofluorescence and Terminal Deoxynucleotidyl Transferase-mediated dUTP Nick-end Labeling Assays

A spinal cord segment, 0.5 cm in length, from where the injured site was centered was obtained and immobilized using paraformaldehyde. The axial frozen sections (20 μ m) from proximal and distal spinal cords (2 mm away from the center of the injury site) were placed on slides^{38,39}. The tissue sections were first incubated with PFKFB3 (1:100, ab181861, Abcam) and NeuN (1:500, ab104224, Abcam), CC-3 (1:200, ab13847, Abcam), and NeuN or NeuN antibody alone at 4°C overnight, respectively. Next, the secondary antibodies (1:500, Invitrogen (USA), Thermo Fisher Scientific) and terminal deoxynucleotidyl transferase-mediated dUTP nick-end labeling (TUNEL) dye liquor (Roche Inc., Basel, Switzerland) were each incubated at 25°C for 2 h. Finally, 4',6-diamidino-2-phenylindole (1 μ g/ml, Roche Inc.) was used to dye the nucleus and mount the medium. A fluorescence microscope (Olympus, Tokyo, Japan) was used to observe the tissue sections, and Photoshop 13.0 software (Adobe Systems Inc., San Jose, CA, USA) was used for photo postprocessing. Six sections were

obtained from each sample, and one random field of gray matter was used from each section to count the cell numbers at $\times 200$ magnification.

PFKFB3 expression was conveyed as the mean ratio of PFKFB3-positive neurons to total neurons in each group. Neuronal apoptosis was expressed as the mean ratio of CC-3-/TUNEL-positive neurons to total neurons in each group.

Measurement of Lactic Acid Levels

The detection of tissue lactic acid content was conducted using the Lactic Acid Assay Kit (JianCheng Bioengineering Institute, Nanjing, Jiangsu, China), following the manufacturer's instructions. The fresh tissues were homogenized in 9 \times volume normal saline and centrifuged at 2,500 \times g for 10 min at 4°C. Before conducting lactic acid detection, the supernatant was deproteinized via the trichloroacetic acid (TCA) method using the Deproteinizing Sample Preparation Kit II (Biovision, San Francisco, CA, USA). In brief, a sample of 100 μ l was mixed with 15 μ l of cold TCA, maintained on ice for 15 min, and centrifuged at 12,000 \times g for 15 min at 4°C. The supernatant was mixed with 10 μ l of cold neutralization solution and maintained on ice for 5 min. A 20 μ l sample, 1,000 μ l working solution, and 200 μ l chromogenic reagent were mixed and incubated at 37°C for 10 min. Then, the terminating solution was added to stop the reaction. The absorbance was measured at 530 nm. The results were expressed as mmol of lactic acid per gram of protein. The data were compared with the sham group to acquire the relative lactic acid levels. The assays were repeated three times independently.

Nuclei Isolation

Nuclei were isolated using Nuclear Extraction Kit (Solarbio, Beijing, China), following the manufacturer's instructions. In brief, the fresh tissues were mixed with 1 ml of the lysis buffer and 50 μ l of reagent A and placed into a homogenizer to grind into a tissue homogenate. The suspension was centrifuged at 700 \times g for 5 min at 4°C, and the precipitate was resuspended in 0.5 ml cold lysis buffer. The suspension was then added to 0.5 ml medium buffer in an eppendorf (EP) tube and centrifuged at 700 \times g for 5 min at 4°C. The precipitate was resuspended in 0.5 ml cold lysis buffer again and centrifuged at 1,000 \times g for 10 min at 4°C to acquire pure nuclei⁴⁰.

Measurement of F2,6BP Levels in Cells and Nuclei

The F2,6BP content was determined as previously described⁴¹. Briefly, tissue debris or pure nuclei were lysed in 0.1 M NaOH and incubated at 80°C for 5 min. After centrifugation, the supernatant was used for the F2,6BP assay after being neutralized with ice-cold acetic acid in 20 mmol/l 4-(2-hydroxyethyl)-1-piperazineethanesulfonic

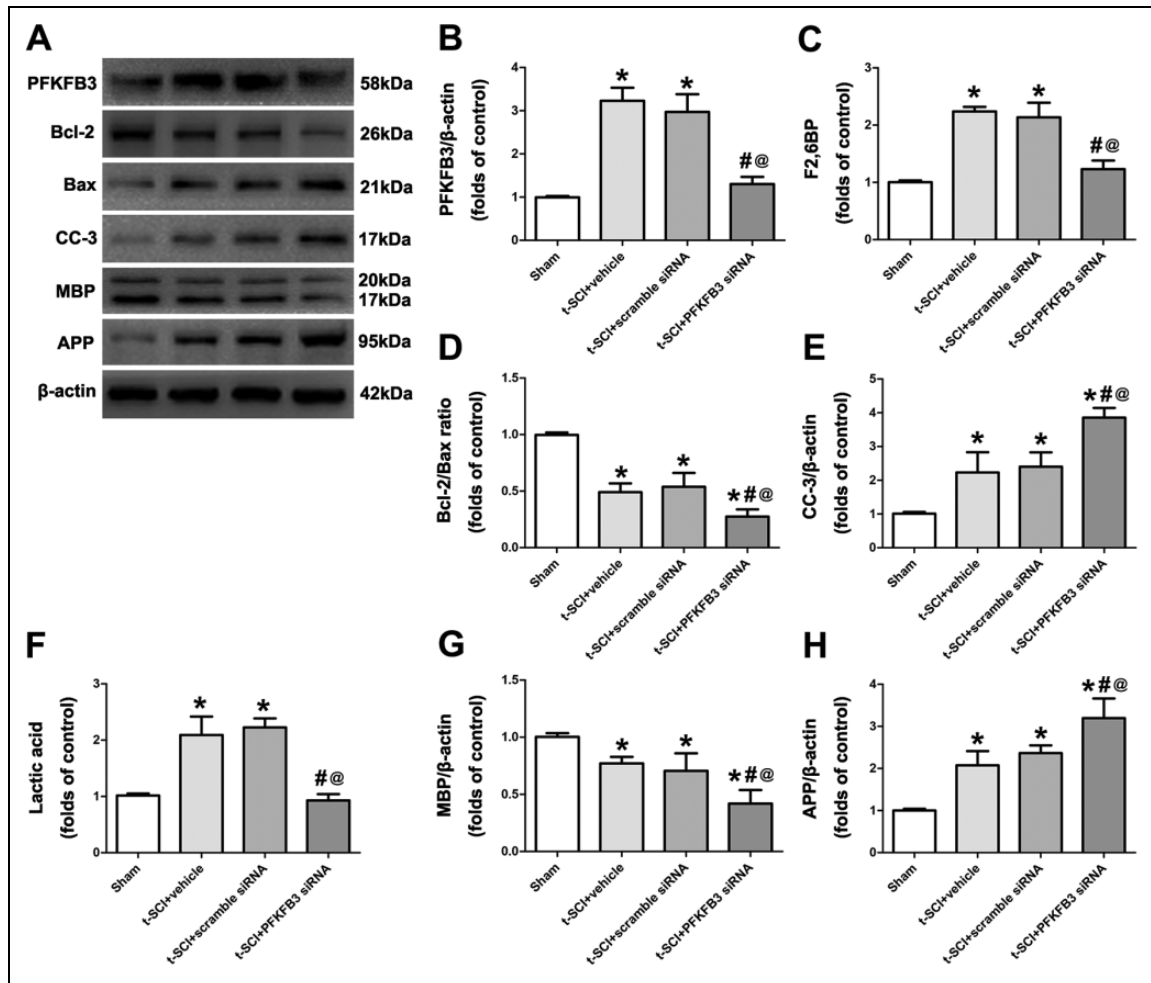


Fig. 2. Knockdown of PFKFB3 decreased F2,6BP and lactic acid, while increased apoptosis and white matter injury at 24 h postinjury. Representative western blot images (A); the levels of PFKFB3 (B); the levels of F2,6BP (C); the Bcl-2/Bax ratio (D); the levels of CC-3 (E); the lactic acid levels (F); the levels of MBP (G); the levels of APP (H). $N = 6$ for each group. Data are expressed as the mean \pm SD. * $P < 0.05$ versus sham; # $P < 0.05$ versus t-SCI + vehicle; @ $P < 0.05$ versus t-SCI + scramble siRNA. F2,6BP: fructose-2,6-bisphosphate; PFKFB3: 6-phosphofructo-2-kinase/fructose-2,6-bisphosphatase; SD: standard deviation; siRNA: small interfering RNA; t-SCI: traumatic spinal cord injury.

acid buffer. The supernatant was added into the mixture containing 50 mmol/l Tris/HCl (pH 8.0), 5 mmol/l $MgCl_2$, 0.15 mmol/l NADH, 17.5 mmol/l glucose-6-phosphate, 0.5 mmol/l pyrophosphate, 1 mmol/l fructose 6-phosphate, 50 μ g/ml aldolase, 1 μ g/ml triosephosphate isomerase, and 10 μ g/ml glycerol-3-phosphate dehydrogenase and was incubated at 25°C for 2 min. The absorbance was measured at 340 nm. The results were expressed as pmol of F2,6BP per microgram of protein. The data were compared with those of the sham group to acquire the relative F2,6BP levels, and the assays were repeated three times independently.

Detection of CDK1 Activity

CDK1 activity was detected using the MESACUP Cdc2/Cdk1 kinase assay kit (MBL, Nagoya, Japan), according to the manufacturer's instructions. Briefly, the pure nuclei were lysed in 50 μ l of hypotonic lysis buffer on ice for 1

h. After centrifugation, 2.5 μ l of supernatant, 2.5 μ l of 10 \times cdc2 reaction buffers, 2.5 μ l of biotinylated MV peptide, 15 μ l of distilled water, and 2.5 μ l of 1 mmol/l adenosine triphosphate (ATP) were mixed together and incubated at 30°C for 30 min. Then, 100 μ l of phosphorylation terminating reagent was added. After centrifugation, 50 μ l of supernatant was added to the wells of a microplate coated with phosphor-MV peptide antibody, which was then incubated at 25°C for 60 min. After washing, 50 μ l of peroxidase (POD)-streptavidin conjugate was added to each well, which was then incubated at 25°C for 30 min. After washing again, 50 μ l of substrate solution was added to each well, which was incubated at 25°C for 5 min before the terminating reagent was added. The absorbance was measured at 492 nm. The data were compared with those of the sham group to acquire the relative optical density (OD) value⁴². The assays were repeated three times independently.

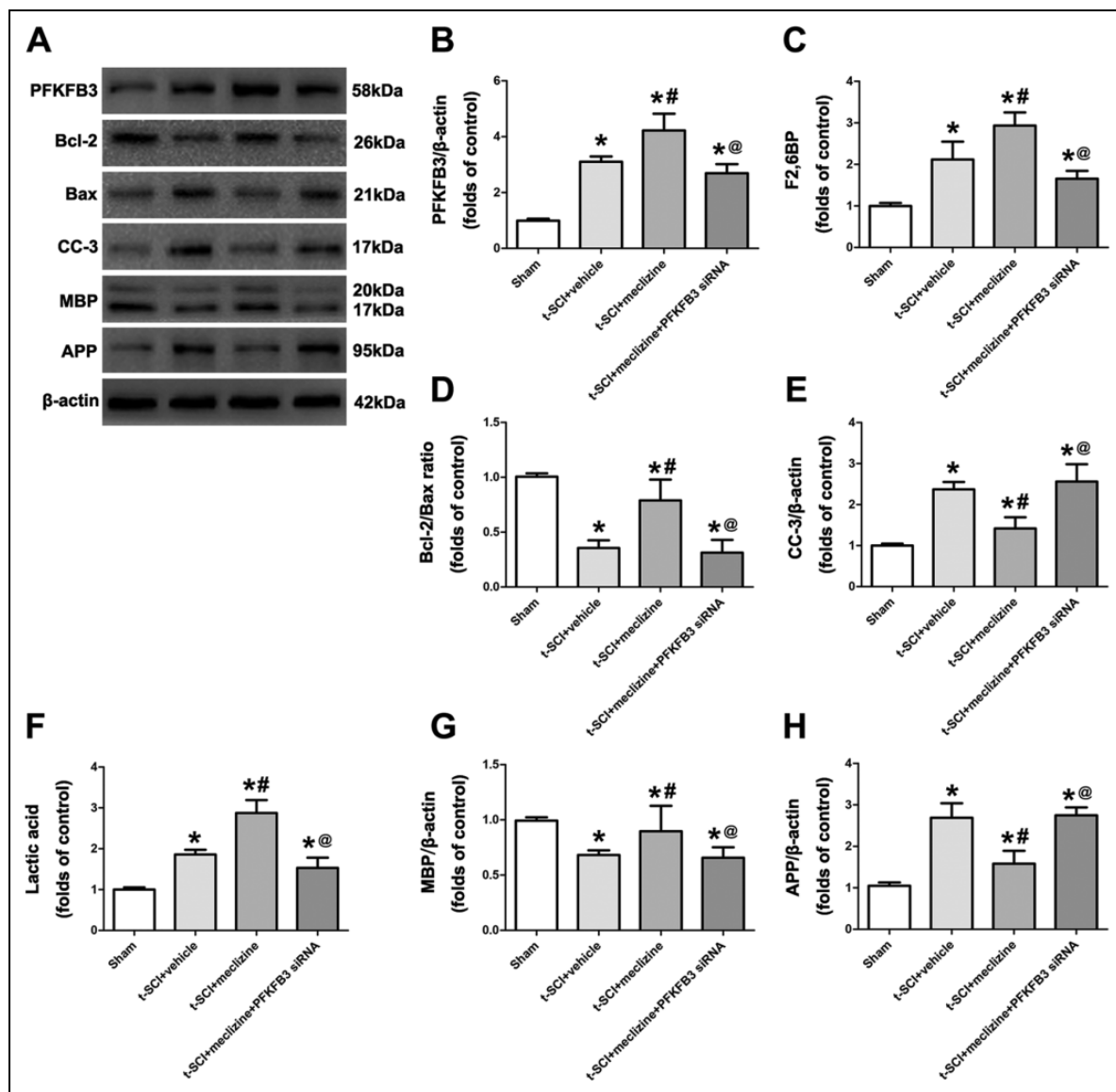


Fig. 3. Meclizine increased PFKFB3, F2,6BP, and lactic acid, while decreased apoptosis and white matter injury at 24 h postinjury. Representative western blot images (A); the levels of PFKFB3 (B); the levels of F2,6BP (C); the Bcl-2/Bax ratio (D); the levels of CC-3 (E); the lactic acid levels (F); the levels of MBP (G); the levels of APP (H). $N = 6$ for each group. Data are expressed as the mean \pm SD. * $P < 0.05$ versus sham; # $P < 0.05$ versus t-SCI + vehicle; @ $P < 0.05$ versus t-SCI + meclizine. F2,6BP: fructose-2,6-bisphosphate; PFKFB3: 6-phosphofructo-2-kinase/fructose-2,6-bisphosphatase; SD: standard deviation; t-SCI: traumatic spinal cord injury.

Transmission Electron Microscopy

A spinal cord segment, 0.5 cm in length, from where the injured site was centered was obtained. The gray matter from the proximal and distal spinal cord (2 mm away from the center of the injury site) were cut into 1 mm³ tissue blocks and fixed overnight in 2.5% glutaraldehyde. Next, the blocks were rinsed, fixated in 1% osmic acid for 1 h, dehydrated in gradient alcohol, and embedded in araldite overnight at 60°C. Finally, the blocks were sectioned into 100 nm ultrathin slices, stained using uranyl acetate and lead citrate, and were then observed using a TEM (Philips Tecnai10, Amsterdam, Holland). Six sections were obtained from each sample, and 10

random neurons per section were used to count the mitochondria around the neuron nucleus at $\times 4,200$ magnification. The mitochondria vacuolization rate refers to the mean ratio of vacuolated to total mitochondria in each group.

Statistical Analysis

The results were presented as mean \pm standard deviation and analyzed by *t*-test, one- or two-way analysis of variance (ANOVA), and Bonferroni's post hoc multiple comparisons test, using $P < 0.05$ as the standard for statistical significance. Statistical analyses were conducted using GraphPad Prism 6 (San Diego, CA, USA).

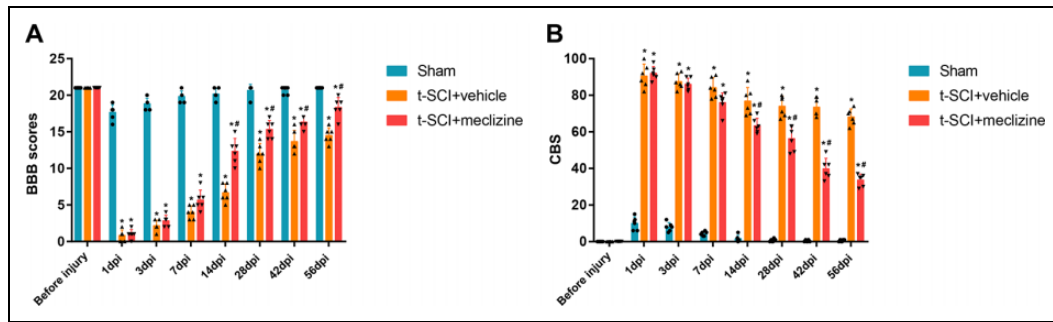


Fig. 4. Meclizine improved motor function of t-SCI rats. The BBB scores (A); the CBS (B). $N = 6$ for each group. Data are expressed as the mean \pm SD. * $P < 0.05$ versus sham; # $P < 0.05$ versus t-SCI + vehicle. BBB: Basso, Beattie, and Bresnahan; dpi: day postinjury; SD: standard deviation; t-SCI: traumatic spinal cord injury.

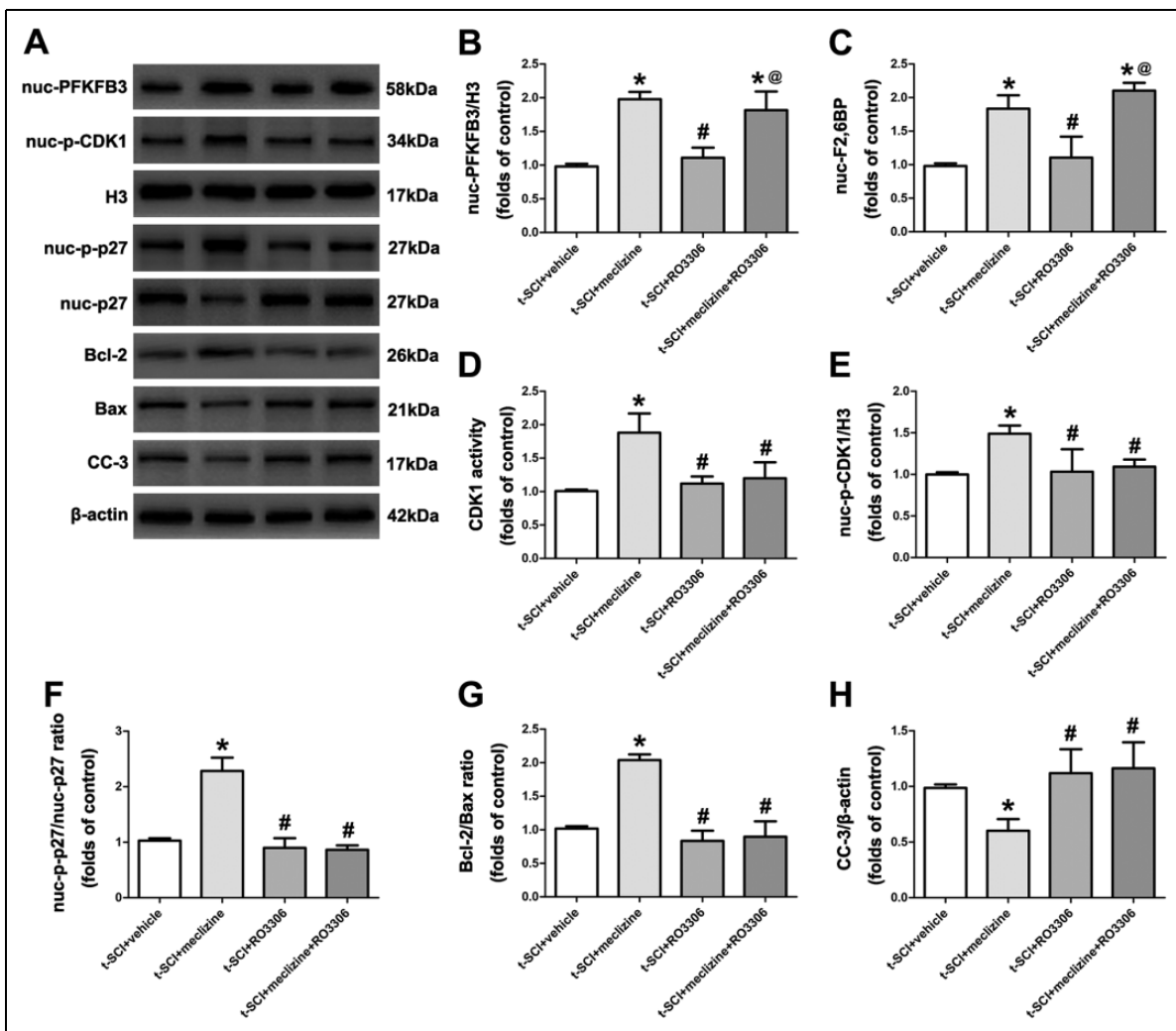


Fig. 5. Meclizine's antiapoptotic effects were mediated by CDK1 and could be reversed by RO3306 at 24 h postinjury. Representative western blot images (A); the levels of nuc-PFKFB3 (B); the levels of nuc-F2,6BP (C); the CDK1 activities (D); the levels of nuc-p-CDK1 (E); the nuc-p-p27/nuc-p27 ratio (F); the Bcl-2/Bax ratio (G); and the levels of CC-3 (H). $N = 6$ for each group. Data are expressed as the mean \pm SD. * $P < 0.05$ versus t-SCI + vehicle; # $P < 0.05$ versus t-SCI + meclizine; @ $P < 0.05$ versus t-SCI + RO3306. CDK1: cyclin-dependent kinase 1; F2,6BP: fructose-2,6-bisphosphate; PFKFB3: 6-phosphofructo-2-kinase/fructose-2,6-bisphosphatase; SD: standard deviation; t-SCI: traumatic spinal cord injury.

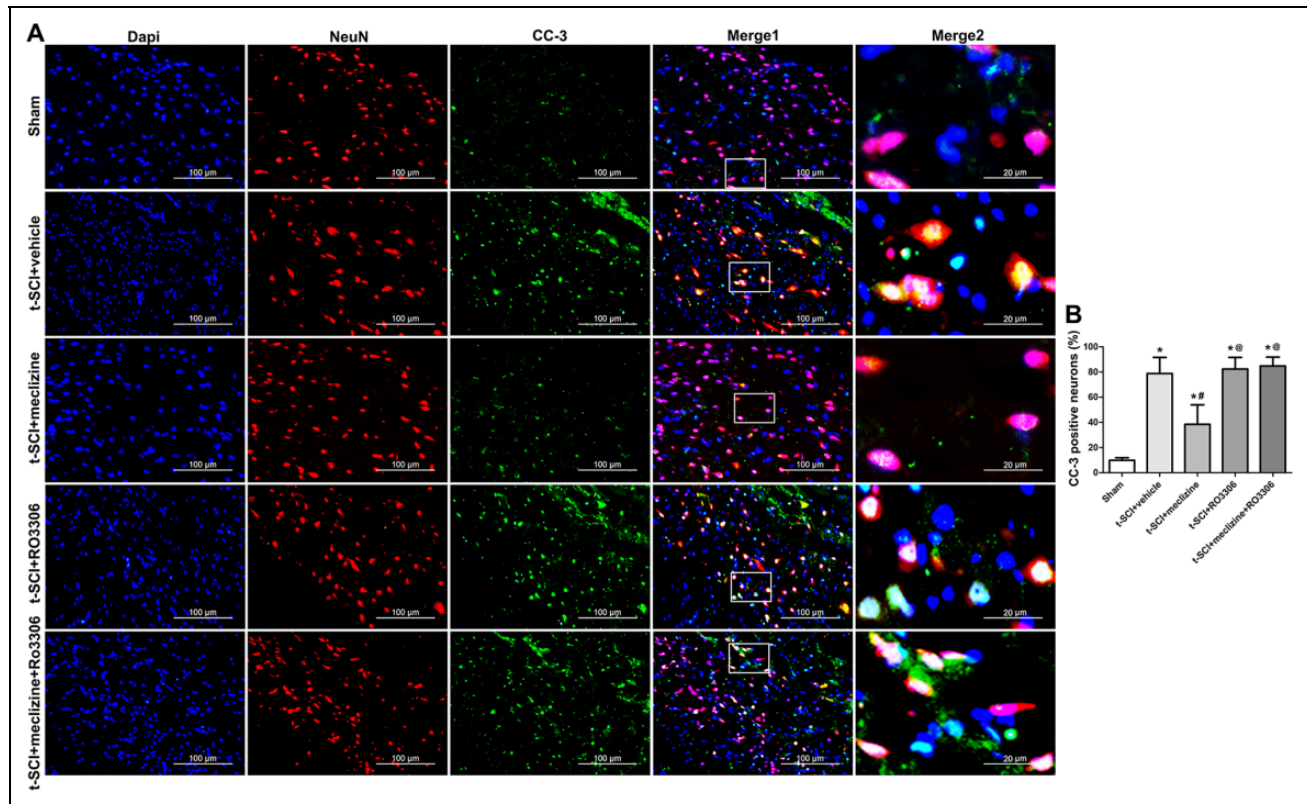


Fig. 6. Meclizine's antiapoptotic effects were reversed by RO3306 at 24 h postinjury. Representative microphotographs of double immunofluorescence staining of CC-3 and NeuN (A); the proportion of CC-3-positive neurons (B). Data are expressed as mean \pm SD. * $P < 0.05$ versus t-SCI + vehicle; # $P < 0.05$ versus t-SCI + meclizine; ® $P < 0.05$ versus t-SCI + RO3306. SD: standard deviation; t-SCI: traumatic spinal cord injury.

Results

Time Course of FBKFB3 and F2,6BP

PFKFB3 level began increasing significantly at 6 h following t-SCI, reaching its peak at 24 h, compared to the sham group ($P < 0.05$). The PFKFB3 level then gradually decreased at 48 and 72 h following t-SCI, compared to the t-SCI 24 h group ($P < 0.05$, Fig. 1B, C). Interestingly, the F2,6BP levels exhibited similar trends (Fig. 1D).

Expression of FBKFB3 in Neurons 24 h After t-SCI

PFKFB3 was expressed in both the nucleus and cytoplasm of neurons. The t-SCI 24 h group had a higher proportion of PFKFB3-positive neurons than the sham group ($P < 0.05$, Fig. 1E, F).

Knockdown of PFKFB3 Decreased Lactic Acid Levels and Increased Apoptosis and White Matter Injury 24 h After t-SCI

When compared to the sham group ($P < 0.05$), the t-SCI + vehicle group had significantly elevated levels of PFKFB3, F2,6BP, lactic acid, CC-3, and APP, but the Bcl-2/Bax ratio and the level of MBP were significantly decreased. PFKFB3

siRNA significantly decreased the PFKFB3, F2,6BP, lactic acid, and MBP levels, as well as the Bcl-2/Bax ratio, but increased the levels of CC-3 and APP, compared to the t-SCI + vehicle group ($P < 0.05$). In addition, the scramble siRNA did not alter the PFKFB3 levels, nor its downstream molecules compared to the t-SCI + vehicle group ($P > 0.05$, Fig. 2A–H).

Upregulation of PFKFB3 Increased Lactic Acid and Reduced Apoptosis and White Matter Injury 24 h After t-SCI

Meclizine significantly increased the PFKFB3, F2,6BP, lactic acid, and MBP levels, as well as the Bcl-2/Bax ratio, but decreased the levels of CC-3 and APP, compared to the t-SCI + vehicle group ($P < 0.05$). Moreover, the combined treatment with PFKFB3 siRNA significantly reversed the effects of meclizine ($P < 0.05$ t-SCI + meclizine versus t-SCI + meclizine + PFKFB3 siRNA, Fig. 3A–H).

Meclizine Improved Motor Function

The BBB scores slightly decreased on the first day but rapidly returned to near-baseline levels in the sham group.

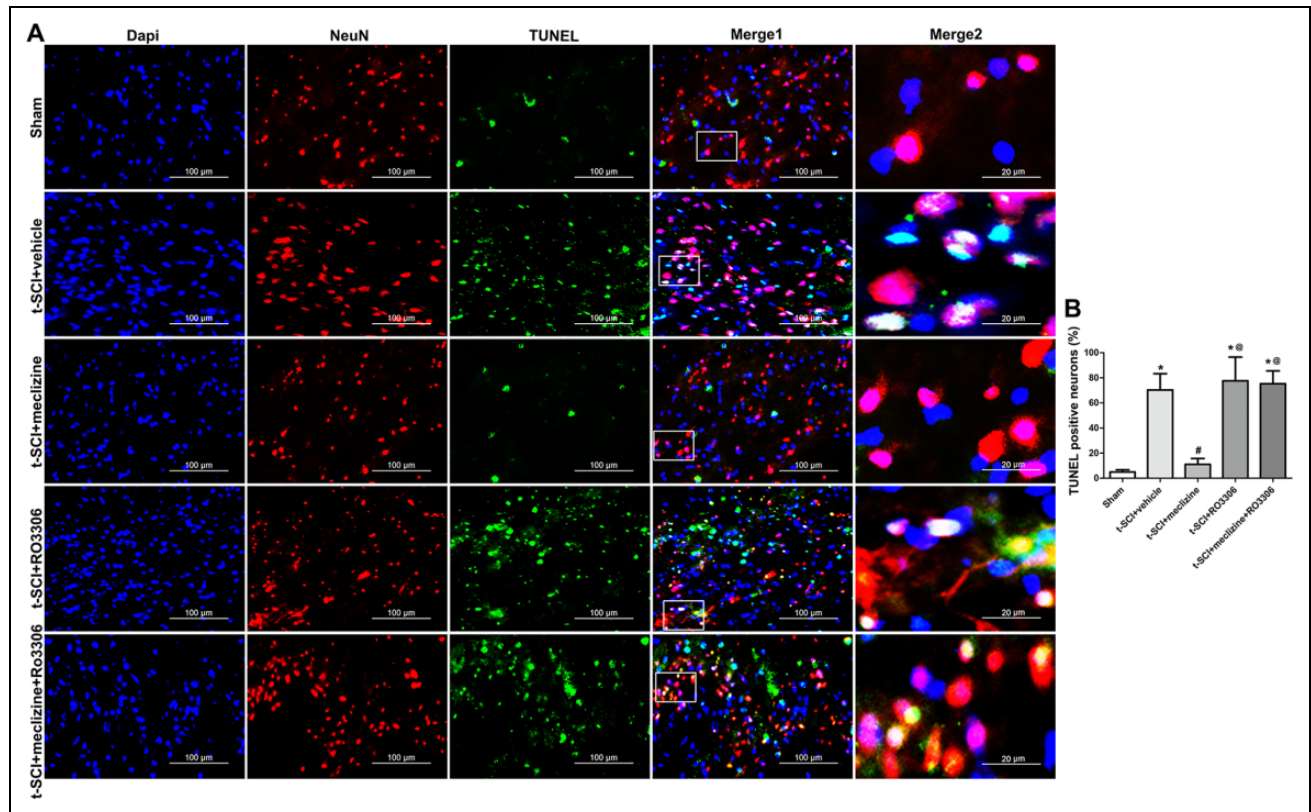


Fig. 7. Meclizine's antiapoptotic effects were reversed by RO3306 at 24 h postinjury. Representative microphotographs of double immunofluorescence staining of TUNEL and NeuN (A); the proportion of TUNEL-positive neurons (B). $N = 6$ for each group. Data are expressed as mean \pm SD. * $P < 0.05$ versus t-SCI + vehicle; # $P < 0.05$ versus t-SCI + meclizine; @ $P < 0.05$ versus t-SCI + RO3306. SD: standard deviation; t-SCI: traumatic spinal cord injury; TUNEL: terminal deoxynucleotidyl transferase-mediated dUTP nick-end labeling.

However, the BBB scores in the t-SCI + vehicle group and the t-SCI + meclizine group decreased to almost 0 on the first day after t-SCI, which were significantly lower than those in the sham group ($P < 0.05$). As observations continued, the BBB scores gradually increased in these two groups but were still significantly lower than those in the sham group ($P < 0.05$). On the 14th day and subsequent periods of observation, the BBB scores in the t-SCI + meclizine group showed a marked increase compared to those in the t-SCI + vehicle group ($P < 0.05$, Fig. 4A).

The CBS of the sham group slightly increased on the first day, but rapidly returned to a score near 0. However, the CBS in both the t-SCI + vehicle group and the t-SCI + meclizine group increased to a score of approximately 100 on the first day after t-SCI, which was noticeably higher than the scores in the sham group ($P < 0.05$). As observations continued, CBS gradually decreased in these two groups but were still evidently higher than those in the sham group ($P < 0.05$). Meclizine significantly increased CBS on the 14th day and the subsequent observation points when compared to the t-SCI + vehicle group ($P < 0.05$, Fig. 4B).

Role of CDK1 in the Meclizine-mediated Antiapoptotic Effects 24 h After t-SCI

Meclizine significantly increased the levels of nuc-PFKFB3 and nuc-F2,6BP compared to the t-SCI + vehicle group ($P < 0.05$). The combined treatment with RO3306 did not alter the levels of nuc-PFKFB3 and nuc-F2,6BP ($P > 0.05$). The CDK1 activity, the level of nuc-p-CDK1, the nuc-p-p27/nuc-p27 ratio, and the Bcl-2/Bax ratio significantly increased, and the level of CC-3 significantly decreased in the t-SCI + meclizine group compared to the t-SCI + vehicle group ($P < 0.05$). However, combined treatment with RO3306 reversed these effects ($P < 0.05$ t-SCI + meclizine + RO3306 versus t-SCI + meclizine, Fig. 5A–H).

The proportions of CC-3- and TUNEL-positive neurons significantly increased in the t-SCI + vehicle group as compared to the sham group ($P < 0.05$). Meclizine had the opposite effect and significantly decreased the proportions of CC-3- and TUNEL-positive neurons compared to the t-SCI + vehicle group ($P < 0.05$). The combined treatment with RO3306 reversed these effects ($P < 0.05$ t-SCI + meclizine + RO3306 versus t-SCI + meclizine, Figs. 6 and 7).

Electron microscopy showed that the nuclei and mitochondria in the neurons of the sham group appeared normal.

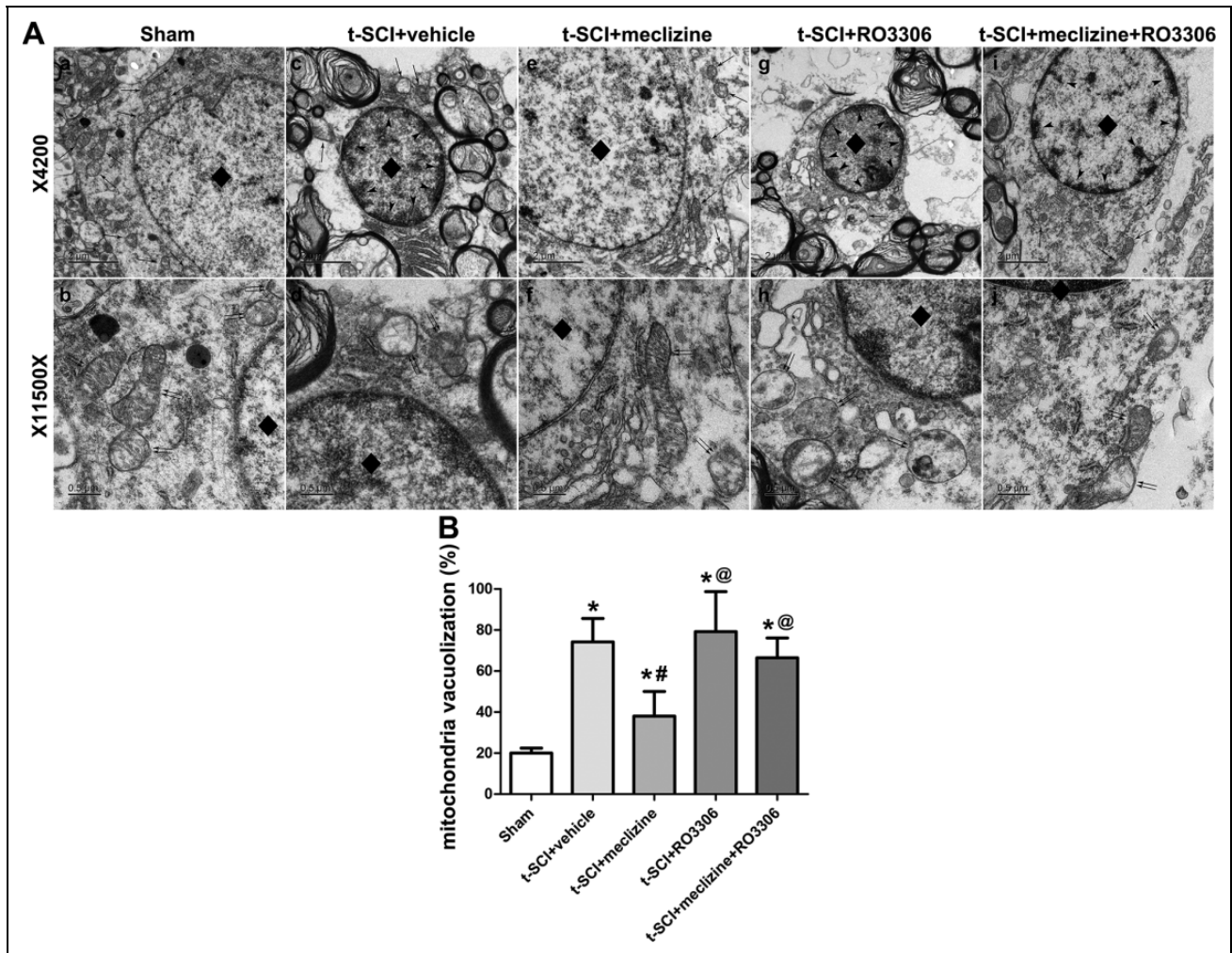


Fig. 8. Meclizine's antiapoptotic effects were reversed by RO3306 at 24 h postinjury. Representative microphotographs of TEM showing nuclei (diamonds), mitochondria ($\times 4,200$, arrow), and mitochondria ($\times 11,500$, double arrow) (A); the proportion of mitochondrial vacuolization (B). $N = 6$ for each group. Data are expressed as the mean \pm SD. * $P < 0.05$ versus t-SCI + vehicle; # $P < 0.05$ versus t-SCI + meclizine; @ $P < 0.05$ versus t-SCI + RO3306. SD: standard deviation; t-SCI: traumatic spinal cord injury; TEM: transmission electron microscopy.

However, the neurons in the t-SCI + vehicle group displayed abnormal ultrastructure, including karyopyknosis, chromatin condensation, and margination, as well as swelling, vacuolization, and reduction of mitochondria. Meclizine recovered the normal ultrastructure, while combined treatment with RO3306 reversed the effects of meclizine. In the t-SCI + vehicle group, the proportions of mitochondrial vacuolization significantly increased when compared to the sham group ($P < 0.05$) and decreased by meclizine ($P < 0.05$). Combined treatment with RO3306 significantly reversed the effects of meclizine ($P < 0.05$, Fig. 8A, B).

Discussion

In this study, we investigated the role of PFKFB3 in the context of t-SCI and further explored the underlying mechanism. The major findings were: (1) the level of

neuronal PFKFB3 significantly increased and peaked at 24 h after t-SCI; (2) knockdown of PFKFB3 inhibited glycolysis and aggravated neuronal apoptosis and white matter injury, while pharmacological activation of PFKFB3 with meclizine significantly enhanced glycolysis and attenuated t-SCI and neurological impairment; (3) meclizine activated CDK1 and promoted the phosphorylation of p27; and (4) pharmacological inhibition of CDK1 reversed the meclizine-mediated antiapoptotic effect under t-SCI conditions. Based on this evidence, PFKFB3 was found to contribute robust neuroprotection against t-SCI by enhancing glycolysis and modulating CDK1-related antiapoptotic signals (Fig. 9).

Apoptosis, characterized by distinctive morphologic changes, such as cell shrinkage, nuclear fragmentation, chromatin condensation, and chromosomal DNA fragmentation, is a programmed cell death process that has been proven to

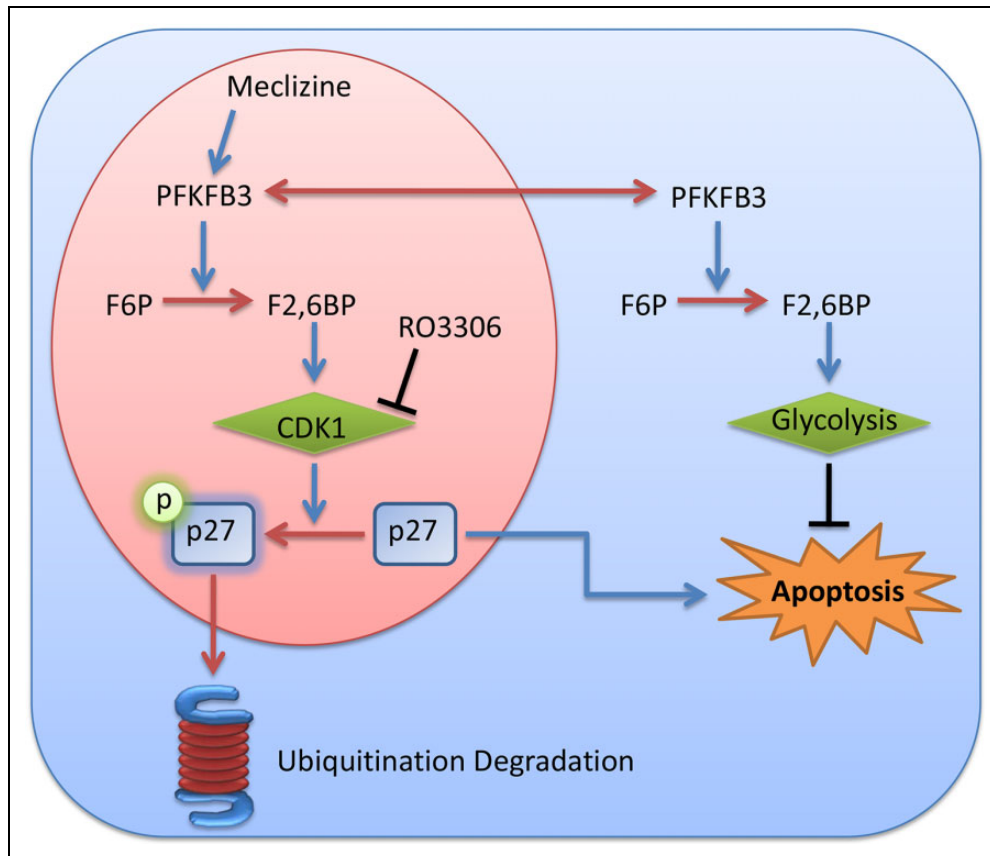


Fig. 9. The signaling map showed the potential molecular mechanisms of meclizine's antiapoptotic effects.

be a critical pathological mechanism accounting for the poor outcome of multiple human diseases, such as heart failure, pulmonary fibrosis, and liver injury⁴³⁻⁴⁵. Additionally, recent studies have demonstrated that targeting apoptosis is beneficial for several acute and chronic CNS diseases, including cerebral ischemia, intracerebral hemorrhage, and Alzheimer's disease^{46,47}. Despite the great efforts that have been made, the exact mechanism of apoptosis has not yet been fully elucidated. Notably, recent studies have revealed an important role of PFKFB3, a critical regulator for glycolysis and metabolism, in the pathological process of apoptosis. The PFKFB3 protein is expressed extensively in human tissues, such as the heart, kidneys, intestines, and spinal cord¹⁷. The activated PFKFB3 can upregulate the activity of F2,6BP, which further activates PFK1, resulting in enhanced glycolysis⁴⁸. Increased glycolysis may confer a beneficial effect for cellular survival via multiple mechanisms, including increasing energy supplements, inhibiting the production of reactive oxygen species, and maintaining the biofunction of voltage-dependent anion channels⁴⁹⁻⁵¹. Notably, the upregulation of glycolysis has been proven to exert a robust neuroprotective effect in ischemic stroke and Alzheimer's disease (AD)^{52,53}. Despite the beneficial effect of PFKFB3 being studied for years, little is known regarding its role in the pathological process of t-SCI.

Therefore, in the first part of this study, we explored the temporal pattern of PFKFB3 after t-SCI. Additionally, similar to a previous study reporting an upregulated level of PFKFB3 after endotoxemia-induced myocardial injury⁵⁴, we observed significant activation of PFKFB3, evidenced by increased PFKFB3 expression and upregulated levels of its substrate F2,6BP, after t-SCI. We then further investigated the effect of PFKFB3 under t-SCI conditions. We found that, consistent with a previous study⁵⁵, inhibition of PFKFB3 significantly inhibited glycolysis (evidenced by the downregulated level of lactic acid), which was accompanied by decreased levels of Bcl-2/Bax and MBP, as well as increased CC-3 and APP expression. Additionally, we noted that activation of PFKFB3 with meclizine remarkably promoted glycolysis, as reported⁵⁶, and meclizine exerted significant neuroprotective effects by attenuating t-SCI-induced neuronal apoptosis and white matter injury. This suggests a critical role of PFKFB3 in regulating glycolysis-related apoptosis under t-SCI conditions, which is a similar result to that which has previously been reported.

Notably, other than regulating glycolysis, recent studies have revealed that PFKFB3 can exert antiapoptotic effects via a glycolysis-independent pattern. The increased F2,6BP levels, which were induced by PFKFB3, could translocate

into nuclei. Therefore, the nuclear F2,6BP could activate CDK1 and subsequently promote the phosphorylation and ubiquitination degradation of p27, a critical initiator to apoptosis, leading to the prevention of cellular apoptosis. Multiple molecular events may cause the enhancement of CDK1 activity, thus, promoting the cell cycle, while the inhibition of CDK1 leads to cell cycle arrest and apoptosis⁵⁷. p27 is considered a tumor suppressor protein due to its effects on regulating the cell cycle and promoting apoptosis in cancer⁵⁸. Meanwhile, p27 also showed antiapoptotic effects in diverse cells and tissues, including neurons⁵⁹. Alessandrini et al. found that p27 phosphorylation on Thr187 was regulated by CDK1 during *in vitro* experiments pertaining to the cell cycle⁶⁰, and the CDK1-mediated phosphorylation of p27 was found to be required for its ubiquitination degradation, which inhibits its apoptosis-promoting effect. Montagnoli et al. found that a stable formation of a trimeric complex, including the cyclin and CDK subunits, was also required for its ubiquitination degradation, with the exception of p27⁶¹. Consistent with previous studies, we found that the activation of PFKFB3 with meclizine significantly increased the level of nuclear PFKFB3 and CDK1. Moreover, consistent with a previous study⁶², our data demonstrated that increased nuclear CDK1 was accompanied by the enhanced phosphorylation of p27, as well as downregulated cellular apoptosis (evidenced by increased proportions of caspase-3-positive cells, TUNEL-positive cells, and abnormal ultrastructures). However, all of the antiapoptotic effects of meclizine against t-SCI were reversed by the CDK1 antagonist RO3306, suggesting a vital role of CDK1 in meclizine-mediated neuroprotective effects via modulating neuronal apoptosis.

Limitations

There were some limitations in our study. First, this study only focused on antiapoptotic effects of PFKFB3 without investigation of its other roles, such as autophagy, insulin signaling, and inflammatory roles, which should be further explored. Second, the antiapoptotic pathway of PFKFB3 in this study was limited to glycolysis enhancement and CDK1-related p27 phosphorylation; further studies on the relationship of PFKFB3 and other signal pathways in neuronal apoptosis after t-SCI are also required.

Conclusions

Our data support that the pharmacological activation of PFKFB3 with meclizine conferred a robust beneficial effect against t-SCI by suppressing neuronal apoptosis and reducing white matter injury. The mechanisms are possibly mediated by enhancing glycolysis and modulating CDK1-related antiapoptotic signals. Our data support that targeting PFKFB3 may be a novel and promising therapeutic strategy for t-SCI.

Ethics Approval

The protocol was approved by the ethics committee of Zhejiang University.

Statement of Human and Animal Rights

All of the experimental procedures involving animals were conducted in accordance with the Ethics Committee of Zhejiang University, China and were performed in compliance with the NIH guidelines for the Care and Use of Laboratory Animals.

Statement of Informed Consent

There are no human subjects in this article and informed consent is not applicable.

Declaration of Conflicting Interests

The author(s) declared no potential conflicts of interest with respect to the research, authorship, and/or publication of this article.

Funding

The author(s) disclosed receipt of the following financial support for the research, authorship, and/or publication of this article: This work was supported by the National Natural Science Foundation of China (Nos. 81870908, 81571106), and the project was cosponsored by the Key Research and Development Programs of Zhejiang Province (No. 2018C03011).

ORCID iD

Gao Chen,  <https://orcid.org/0000-0003-1085-0028>

References

1. Donovan J, Kirshblum S. Clinical trials in traumatic spinal cord injury. *Neurotherapeutics*. 2018;15(3):654–668.
2. Bartus K, Galino J, James ND, Hernandez-Miranda LR, Dawes JM, Fricker FR, Garratt AN, McMahon SB, Ramer MS, Birchmeier C, Bennett DL, et al. Neuregulin-1 controls an endogenous repair mechanism after spinal cord injury. *Brain*. 2016; 139(Pt 5):1394–1416.
3. Papa S, Vismara I, Mariani A, Barilani M, Rimondo S, De Paola M, Panini N, Erba E, Mauri E, Rossi F, Forloni G, et al. Mesenchymal stem cells encapsulated into biomimetic hydrogel scaffold gradually release ccl2 chemokine *in situ* preserving cytoarchitecture and promoting functional recovery in spinal cord injury. *J Control Release*. 2018;278:49–56.
4. Nori S, Ahuja CS, Fehlings MG. Translational advances in the management of acute spinal cord injury: what is new? What is hot? *Neurosurgery*. 2017;64(CN_suppl_1):119–128.
5. Anwar MA, Al Shehabi TS, Eid AH. Inflammogenesis of secondary spinal cord injury. *Front Cell Neurosci*. 2016;10:98.
6. Hagg T, Oudega M. Degenerative and spontaneous regenerative processes after spinal cord injury. *J Neurotrauma*. 2006; 23(3–4):264–280.
7. Fitch MT, Silver J. Cns injury, glial scars, and inflammation: inhibitory extracellular matrices and regeneration failure. *Exp Neurol*. 2008;209(2):294–301.
8. Gaudet AD, Popovich PG. Extracellular matrix regulation of inflammation in the healthy and injured spinal cord. *Exp Neurol*. 2014;258:24–34.

9. Sun X, Jones ZB, Chen XM, Zhou L, So KF, Ren Y. Multiple organ dysfunction and systemic inflammation after spinal cord injury: a complex relationship. *J Neuroinflammation*. 2016; 13(1):260.
10. Ramer LM, Ramer MS, Bradbury EJ. Restoring function after spinal cord injury: towards clinical translation of experimental strategies. *Lancet Neurol*. 2014;13(12):1241–1256.
11. Elizei SS, Kwon BK. The translational importance of establishing biomarkers of human spinal cord injury. *Neural Regen Res*. 2017;12(3):385–388.
12. Pegoraro C, Maczkowiak F, Monsoro-Burq AH. Pfkfb (6-phosphofructo-2-kinase/fructose-2,6-bisphosphatase) isoforms display a tissue-specific and dynamic expression during xenopus laevis development. *Gene Expr Patterns*. 2013;13(7):203–211.
13. Rider MH, Bertrand L, Vertommen D, Michels PA, Rousseau GG, Hue L. 6-phosphofructo-2-kinase/fructose-2,6-bisphosphatase: head-to-head with a bifunctional enzyme that controls glycolysis. *Biochem J*. 2004;381(Pt 3):561–579.
14. Chesney J, Mitchell R, Benigni F, Bacher M, Spiegel L, Al-Abed Y, Han JH, Metz C, Bucala R. An inducible gene product for 6-phosphofructo-2-kinase with an au-rich instability element: role in tumor cell glycolysis and the Warburg effect. *Proc Natl Acad Sci U S A*. 1999;96(6):3047–3052.
15. Atsumi T, Chesney J, Metz C, Leng L, Donnelly S, Makita Z, Mitchell R, Bucala R. High expression of inducible 6-phosphofructo-2-kinase/fructose-2,6-bisphosphatase (ipfk-2; pfkfb3) in human cancers. *Cancer Res*. 2002;62(20):5881–5887.
16. Kessler R, Eschrich K. Splice isoforms of ubiquitous 6-phosphofructo-2-kinase/fructose-2,6-bisphosphatase in human brain. *Brain Res Mol Brain Res*. 2001;87(2):190–195.
17. Kessler R, Bleichert F, Warnke JP, Eschrich K. 6-phosphofructo-2-kinase/fructose-2,6-bisphosphatase (pfkfb3) is up-regulated in high-grade astrocytomas. *J Neurooncol*. 2008; 86(3):257–264.
18. Seo M, Kim JD, Neau D, Sehgal I, Lee YH. Structure-based development of small molecule pfkfb3 inhibitors: a framework for potential cancer therapeutic agents targeting the Warburg effect. *PLoS One*. 2011;6(9):e24179.
19. Hanahan D, Weinberg RA. Hallmarks of cancer: the next generation. *Cell*. 2011;144(5):646–674.
20. Qu J, Lu D, Guo H, Miao W, Wu G, Zhou M. Pfkfb3 modulates glycolytic metabolism and alleviates endoplasmic reticulum stress in human osteoarthritis cartilage. *Clin Exp Pharmacol Physiol*. 2016;43(3):312–318.
21. Lv Y, Zhang B, Zhai C, Qiu J, Zhang Y, Yao W, Zhang C. Pfkfb3-mediated glycolysis is involved in reactive astrocyte proliferation after oxygen-glucose deprivation/reperfusion and is regulated by cdh1. *Neurochem Int*. 2015;91:26–33.
22. Fu W, Shi D, Westaway D, Jhamandas JH. Bioenergetic mechanisms in astrocytes may contribute to amyloid plaque deposition and toxicity. *J Biol Chem*. 2015;290(20):12504–12513.
23. Rodriguez-Rodriguez P, Fernandez E, Almeida A, Bolanos JP. Excitotoxic stimulus stabilizes pfkfb3 causing pentose-phosphate pathway to glycolysis switch and neurodegeneration. *Cell Death Differ*. 2012;19(10):1582–1589.
24. Carpenter KL, Jalloh I, Hutchinson PJ. Glycolysis and the significance of lactate in traumatic brain injury. *Front Neurosci*. 2015;9:112.
25. Murai H, Itoh C, Wagai N, Nakamura T, Yamaura A, Makino H. Local spinal cord glucose utilization and extracellular potassium activity changes after spinal cord injury in rats [in Japanese]. *No To Shinkei*. 1991;43(4):337–342.
26. Yalcin A, Clem BF, Imbert-Fernandez Y, Ozcan SC, Peker S, O’Neal J, Klarer AC, Clem AL, Telang S, Chesney J. 6-phosphofructo-2-kinase (pfkfb3) promotes cell cycle progression and suppresses apoptosis via cdk1-mediated phosphorylation of p27. *Cell Death Dis*. 2014;5(7):e1337.
27. Wang Z, Lee B, Pearce D, Qian S, Wang Y, Zhang Q, Chow MS. Meclizine metabolism and pharmacokinetics: formulation on its absorption. *J Clin Pharmacol*. 2012;52(9):1343–1349.
28. Gohil VM, Sheth SA, Nilsson R, Wojtovich AP, Lee JH, Perocchi F, Chen W, Clish CB, Ayata C, Brookes PS, Mootha VK. Nutrient-sensitized screening for drugs that shift energy metabolism from mitochondrial respiration to glycolysis. *Nat Biotechnol*. 2010;28(3):249–255.
29. Hong CT, Chau KY, Schapira AH. Meclizine-induced enhanced glycolysis is neuroprotective in Parkinson disease cell models. *Sci Rep*. 2016;6:25344.
30. Gohil VM, Offner N, Walker JA, Sheth SA, Fossale E, Gusella JF, MacDonald ME, Neri C, Mootha VK. Meclizine is neuroprotective in models of Huntington’s disease. *Hum Mol Genet*. 2011;20(2):294–300.
31. Liang W, Han Q, Jin W, Xiao Z, Huang J, Ni H, Chen B, Kong J, Wu J, Dai J. The promotion of neurological recovery in the rat spinal cord crushed injury model by collagen-binding bdnf. *Biomaterials*. 2010;31(33):8634–8641.
32. Gao L, Zhang Z, Xu W, Li T, Ying G, Qin B, Li J, Zheng J, Zhao T, Yan F, Zhu Y, et al. Natrium benzoate alleviates neuronal apoptosis via the dj-1-related anti-oxidative stress pathway involving AKT phosphorylation in a rat model of traumatic spinal cord injury. *Front Mol Neurosci*. 2019;12:42.
33. Xu W, Gao L, Li T, Zheng J, Shao A, Zhang J. Apelin-13 alleviates early brain injury after subarachnoid hemorrhage via suppression of endoplasmic reticulum stress-mediated apoptosis and blood-brain barrier disruption: Possible involvement of atf6/chop pathway. *Neuroscience*. 2018;388:284–296.
34. Wu CX, Wang XQ, Chok SH, Man K, Tsang SHY, Chan ACY, Ma KW, Xia W, Cheung TT. Blocking cdk1/pdk1/beta-catenin signaling by cdk1 inhibitor ro3306 increased the efficacy of sorafenib treatment by targeting cancer stem cells in a preclinical model of hepatocellular carcinoma. *Theranostics*. 2018; 8(14):3737–3750.
35. Gao L, Xu W, Fan S, Li T, Zhao T, Ying G, Zheng J, Li J, Zhang Z, Yan F, Zhu Y, et al. Manf attenuates neuronal apoptosis and promotes behavioral recovery via akt/mdm-2/p53 pathway after traumatic spinal cord injury in rats. *Biofactors*. 2018;44(4):369–386.
36. Hylden JL, Wilcox GL. Intrathecal morphine in mice: a new technique. *Eur J Pharmacol*. 1980;67(2–3):313–316.

37. Kang S, Liu S, Li H, Wang D, Qi X. Baicalin effects on rats with spinal cord injury by anti-inflammatory and regulating the serum metabolic disorder. *J Cell Biochem.* 2018;119(9):7767–7779.
38. Kjell J, Olson L, Abrams MB. Improved recovery from spinal cord injury in rats with chronic parvovirus serotype-1a infection. *Spinal Cord.* 2016;54(7):517–520.
39. Wang S, Liu Y, Wu C, Zhao W, Zhang J, Bao G, Xu G, Sun Y, Chen J, Cui Z. The expression of igfbp6 after spinal cord injury: implications for neuronal apoptosis. *Neurochem Res.* 2017;42(2):455–467.
40. Yalcin A, Clem BF, Simmons A, Lane A, Nelson K, Clem AL, Brock E, Siow D, Wattenberg B, Telang S, Chesney J. Nuclear targeting of 6-phosphofructo-2-kinase (pfkfb3) increases proliferation via cyclin-dependent kinases. *J Biol Chem.* 2009;284(36):24223–24232.
41. Van Schaftingen E, Lederer B, Bartrons R, Hers HG. A kinetic study of pyrophosphate: fructose-6-phosphate phosphotransferase from potato tubers. Application to a microassay of fructose 2,6-bisphosphate. *Eur J Biochem.* 1982;129(1):191–195.
42. Prasad S, Koch B, Chaube SK. Ro-3306 prevents postovulatory aging-mediated spontaneous exit from m-ii arrest in rat eggs cultured in vitro. *Biomed Pharmacother.* 2016;78:216–225.
43. Hou X, Fu M, Cheng B, Kang Y, Xie D. Galanthamine improves myocardial ischemia-reperfusion-induced cardiac dysfunction, endoplasmic reticulum stress-related apoptosis, and myocardial fibrosis by suppressing ampk/nrf2 pathway in rats. *Ann Transl Med.* 2019;7(22):634.
44. Larson-Casey JL, He C, Carter AB. Mitochondrial quality control in pulmonary fibrosis. *Redox Biol.* 2020;33:101426.
45. Xu Q, Shi W, Lv P, Meng W, Mao G, Gong C, Chen Y, Wei Y, He X, Zhao J, Han H, et al. Critical role of caveolin-1 in aflatoxin b1-induced hepatotoxicity via the regulation of oxidation and autophagy. *Cell Death Dis.* 2020;11(1):6.
46. Li X, Wu X, Luo P, Xiong L. Astrocyte-specific ndrg2 gene: functions in the brain and neurological diseases. *Cell Mol Life Sci.* 2019;77(13):2461–2472.
47. Martinelli C, Pucci C, Battaglini M, Marino A, Ciofani G. Antioxidants and nanotechnology: promises and limits of potentially disruptive approaches in the treatment of central nervous system diseases. *Adv Healthc Mater.* 2019;9(3):e1901589.
48. Wang J, Guan H, Liu H, Lei Z, Kang H, Guo Q, Dong Y, Liu H, Sun Y, Fang Z, Li F. Inhibition of pfkfb3 suppresses osteoclastogenesis and prevents ovariectomy-induced bone loss. *J Cell Mol Med.* 2019;24(3):2294–2307.
49. Gottlob K, Majewski N, Kennedy S, Kandel E, Robey RB, Hay N. Inhibition of early apoptotic events by akt/pkb is dependent on the first committed step of glycolysis and mitochondrial hexokinase. *Genes Dev.* 2001;15(11):1406–1418.
50. Domenech E, Maestre C, Esteban-Martinez L, Partida D, Pascual R, Fernandez-Miranda G, Seco E, Campos-Olivas R, Perez M, Megias D, Allen K, et al. Ampk and pfkfb3 mediate glycolysis and survival in response to mitophagy during mitotic arrest. *Nat Cell Biol.* 2015;17(10):1304–1316.
51. Archer SL. Acquired mitochondrial abnormalities, including epigenetic inhibition of superoxide dismutase 2, in pulmonary hypertension and cancer: therapeutic implications. *Adv Exp Med Biol.* 2016;903:29–53.
52. Liu W, Mu F, Liu T, Xu H, Chen J, Jia N, Zhang Y, Dou F, Shi L, Li Y, Wen A, et al. Ultra performance liquid chromatography/quadrupole time-of-flight mass spectrometry-based metabolomics reveal protective effect of terminalia chebula extract on ischemic stroke rats. *Rejuvenation Res.* 2018;21(6):541–552.
53. Williams HC, Farmer BC, Piron MA, Walsh AE, Bruntz R, Gentry M, Sun RC, Johnson LA. Apoe alters glucose flux through central carbon pathways in astrocytes. *Neurobiol Dis.* 2020;136:104742.
54. Tian W, Guo HS, Li CY, Cao W, Wang XY, Mo D, Hao XW, Feng YD, Sun Y, Lei F, Zhang HN, et al. Pfkfb3 promotes endotoxemia-induced myocardial dysfunction through inflammatory signaling and apoptotic induction. *Toxicol Appl Pharmacol.* 2019;368:26–36.
55. Miyagawa K, Shi M, Chen PI, Hennigs JK, Zhao Z, Wang M, Li CG, Saito T, Taylor S, Sa S, Cao A, et al. Smooth muscle contact drives endothelial regeneration by bmp2-notch1-mediated metabolic and epigenetic changes. *Circ Res.* 2019;124(2):211–224.
56. Bartrons R, Rodriguez-Garcia A, Simon-Molas H, Castano E, Manzano A, Navarro-Sabate A. The potential utility of pfkfb3 as a therapeutic target. *Expert Opin Ther Targets.* 2018;22(8):659–674.
57. Shapiro GI. Cyclin-dependent kinase pathways as targets for cancer treatment. *J Clin Oncol.* 2006;24(11):1770–1783.
58. Abbastabar M, Kheyrollah M, Azizian K, Bagherlou N, Tehrani SS, Maniati M, Karimian A. Multiple functions of p27 in cell cycle, apoptosis, epigenetic modification and transcriptional regulation for the control of cell growth: a double-edged sword protein. *DNA Repair (Amst).* 2018;69:63–72.
59. Jaiswal S, Sharma P. Role and regulation of p27 in neuronal apoptosis. *J Neurochem.* 2017;140(4):576–588.
60. Alessandrini A, Chiaur DS, Pagano M. Regulation of the cyclin-dependent kinase inhibitor p27 by degradation and phosphorylation. *Leukemia.* 1997;11(3):342–345.
61. Montagnoli A, Fiore F, Eytan E, Carrano AC, Draetta GF, Herskho A, Pagano M. Ubiquitination of p27 is regulated by cdk-dependent phosphorylation and trimeric complex formation. *Genes Dev.* 1999;13(9):1181–1189.
62. Garcia-Gutierrez L, Bretones G, Molina E, Arechaga I, Symonds C, Acosta JC, Blanco R, Fernandez A, Alonso L, Sicinski P, Barbacid M, et al. Myc stimulates cell cycle progression through the activation of cdk1 and phosphorylation of p27. *Sci Rep.* 2019;9(1):18693.